Hindawi
Journal of Sensors
Volume 2024, Article ID 6696108, 10 pages
https://doi.org/10.1155/2024/6696108

Research Article

Effect of Electrode Shape on the Performance of ZnO-Based Ethanol Sensor

Shokoufeh Sirjani,[1] **Ali Fattah**,[1] **and Hamid Haratizadeh**[2]

[1]*Electrical Engineering Department, Shahrood University of Technology, Shahrood, Iran*
[2]*Physics Department, Shahrood University of Technology, Shahrood, Iran*

Correspondence should be addressed to Shokoufeh Sirjani; shokoufehsirjani@shahroodut.ac.ir

Received 22 August 2023; Revised 15 March 2024; Accepted 20 March 2024; Published 23 April 2024

Academic Editor: Michele Penza

This paper reports the deposition of Zn on glass substrates using the physical vapor deposition (PVD) method, followed by an annealing process to grow ZnO for gas-sensing applications. Surface morphologies were characterized using scanning electron microscopy, which revealed nanowire shape. The diameter of the wire was about 35 nm. In addition, X-ray diffraction analysis demonstrated that the ZnO nanowire possessed a wurtzite structure with an orientation of (002). Three types of resistive gas sensors with a spiral-square and two-comb electrode geometries were designed, fabricated, and tested for their ethanol vapor-sensing properties. The experimental results show that the sensor with square-spiral electrode has the sensitivity of 43% for 2,000 ppm of ethanol vapor at 200°C, while the sensor with a comb electrode shows the sensitivity of 32% at the same conditions. Also, two sensors with different dimensions of comb-shaped electrodes showed the same sensitivity, as both the width and the distance between the fingers change simultaneously in the larger comb-shaped electrode. The response time for the comb electrode is shorter than the square-spiral type, and the recovery time is almost independent of the electrode geometry. Therefore, the optimal structure should be selected based on the application.

1. Introduction

Nowadays, to detect volatile and toxic gases, according to environmental policies and legislation, as well as the security limits of life and industry, sensor devices have special importance in everyday people's lives [1]. The importance of increasing sensitivity, accuracy, and speed in gas sensors is well known. In recent years, many efforts have been made to achieve high sensitivity of gas sensors in the field of science and engineering, and researchers have tried to achieve this goal using different methods. In this research, changing electrode shape is investigated as a method for increasing sensor sensitivity.

Technological limitations of conventional gas sensors, such as sensitivity, selectivity, or high-temperature performance, have led to the study of new methods, such as using nanostructures in conventional sensing materials. One of the highlight characteristics of nanomaterials is their high surface-to-volume ratio. Nanostructured materials can be used to lower operating temperatures, which reduces power consumption while making their operation safer [2].

Among the gases, ethanol with the molecular formula of C_2H_5OH, molecular weight of 46.07 g/mol, and boiling point of 78.5°C has wide applications in the food industry, pharmaceutical industry, chemical factories, and preventing drunk driving [3, 4]. Normally, exposure to ethanol vapor is not dangerous, but it can lead to headaches, drowsiness, eye irritation, and breathing problems. Therefore, the control of ethanol concentration is particularly important [5]. There are several methods for detecting processes, including gas chromatography, infrared spectroscopy, and electrochemical sensing. However, each method has its limitations. For example, gas chromatography is a highly accurate method but requires expensive equipment and trained personnel. Infrared spectroscopy is a nondestructive method but is not as sensitive as others. Among these methods, metal–oxide semiconductor gas sensors for ethanol detection have attracted widespread attention in recent researches due to their low cost and simple fabrication process. Also, lower selectivity and sensitivity,

high working temperature, and the inability to detect ppb levels of ethanol vapor are the major drawbacks of the metal oxide-based sensors for ethanol-sensing applications. In this research in order to overcome its low sensitivity, a novel method is proposed.

The most common and practical gas sensors are metal–oxide semiconductor types, which have several advantages, such as well stability, high sensitivity, and simple fabrication processes [6]. The working principle of semiconductor gas sensors is based on their resistance variation or conductivity upon exposure to the target gas [7]. This type of gas sensor includes a heater, substrate, sensing material, and electrodes. The heater is placed beneath the substrate which provides the appropriate working temperature of the sensor [8]. One of the common metal–oxide semiconductors is ZnO, which has unique properties and a wide range of applications in thin film transistors, light diodes, and sensors [6]. This material is an n-type semiconductor (oxygen vacancies in the zinc oxide crystal structure often act as an n-type donor) with a hexagonal structure and a wide and direct band gap of about 3.37 eV at room temperature. Due to its high absorption power of ultraviolet light, it is used as a transparent electrode in solar cells and flat screens. In addition, it is used to make gratings in optical electronic devices, as a window material in antireflective coatings and optical filters [9]. The important advantage of ZnO as a sensor material is the ease of making nanostructures such as nanowires, nanotubes, nanobelts, nanospheres, nanoflowers, nanomushrooms, etc. ZnO nanostructures often exhibit favorable sensing performance due to their high specific area [10]. A number of methods have been used for enhancing ZnO performance, such as metal doping [11, 12], deposition method and morphology control [13], effect of working temperature [14, 15], and using multicompositional sensing film [16]. In [13], ZnO was prepared using a simple heat treatment and thermal evaporation technique. The working temperature is observed at 250°C. The sensors were used at concentration ppm ranges of 5–50 at 250°C. The process is based on the ethanol adsorption/desorption, which forms ionic species on the sample surface. The thermal evaporation technique yields to the best sensing response at 250°C. The ethanol-sensing mechanism involves adsorption as a surface defect, forming ionic species on the sample surface. Before gas exposure, oxygen atoms are adsorbed into the ZnO surface, creating a depletion layer. When ethanol vapor is introduced, the depletion layer becomes thinner and reduces the resistance. In [17], the gas mechanism of a ZnO-based ethanol sensor has been discussed. It is well known that the mechanism of n-type metal oxide semiconductors is based on the chemiresistor changes caused by the surface adsorption and desorption of gas molecules.

Also, in this type of sensor, the contact of sensing material with the electrode is Ohmic or Schottky. Electrodes are a part of the semiconductor gas sensor that measures the electrical and catalytic properties of the sensing materials [18]. In addition, the sensing properties of semiconductor gas sensors can be modified using different electrode materials [8, 19–21], electrode geometry [18, 22–24], and electrode placement positions [25, 26]. In [22], the optimization of geometrical parameters of interdigitated electrode structures (finger width, spacing between fingers, and number of fingers) on the methane gas sensor response at different applied voltages has been investigated. The sensor response is found to be more sensitive to variations in finger width than in spacing between them. Also, in [27–29], optimizing the finger distance of the comb electrodes has been investigated to evaluate the response of the gas sensor. In [27], the response of the graphene-based acetone gas sensor was improved by increasing the distance between the electrodes.

The gas-sensing mechanism of the sensor is based on chemisorbed oxygen species and resistance decrement upon the effect of reactions as follows:

$$O_{2(gas)} + e^- \rightleftarrows O_2^-(ads), \quad (1)$$

$$O_{2(gas)} + 2e^- \rightleftarrows 2O^-, \quad (2)$$

$$O^-_{(adsorbed)} + e^- \rightleftarrows O^{2-}, \quad (3)$$

$$C_2H_5OH_{gas} + 3O_2^- \rightleftarrows 2CO_{2(gas)} + 3H_2O + 3e^-, \quad (4)$$

$$C_2H_5OH_{gas} + 6O^- \rightleftarrows 2CO_{2(gas)} + 3H_2O + 6e^-, \quad (5)$$

where (gas) and (ads) denote gas and adsorbate molecules, respectively. Also, Equation (1) relates to the temperature below 200°C, and Equation (2) applies to temperatures ranging from 200 to 300°C. When an n-type semiconductor particle comes into contact with air, it captures the oxygen molecules to its surface and converts them to O_2^-, O^-, and O^{2-}ions. This process occurs by extracting electrons from the conductance band, resulting in the formation of an electron depletion layer near the particle's surface where there are fewer electrons. On the surface of an n-type semiconductor particle, there are three types of oxygen-related substances. As the sensor is exposed to ethanol vapor, it reacts with the O^- ions on the surface, causing the trapped electrons to be released. As a result, the depletion layer becomes thinner, and the resistance of the ZnO layer decreases [30].

Most of the research in the field of sensing has been done on the sensing material, while the role of electrode material, geometry, gap size, and preparation method on the sensing properties of active material have not been fully studied. The electrode material can affect the Ohmic and Schottky properties of the metal-semiconductor junction [30–32]. In this research, the Au electrode and ZnO have Ohmic contacts. Moreover, electrodes can be placed above, below, or on both sides of the sensing layer and the sensitivity of the sensor will change by the variation of electrode position [8, 25, 26]. In [33, 34], the effect of electrode structure on NO_2 gas sensing was investigated. The sensor with spiral electrodes had a better response than a comb one because it has a larger effective surface. Here, the comb structure is chosen and includes the following advantages. This structure increases the effective area. Moreover, the sensitivity could be modified by changing the ratio of finger width to finger distance. Also, comb electrodes are usually made using the photolithography

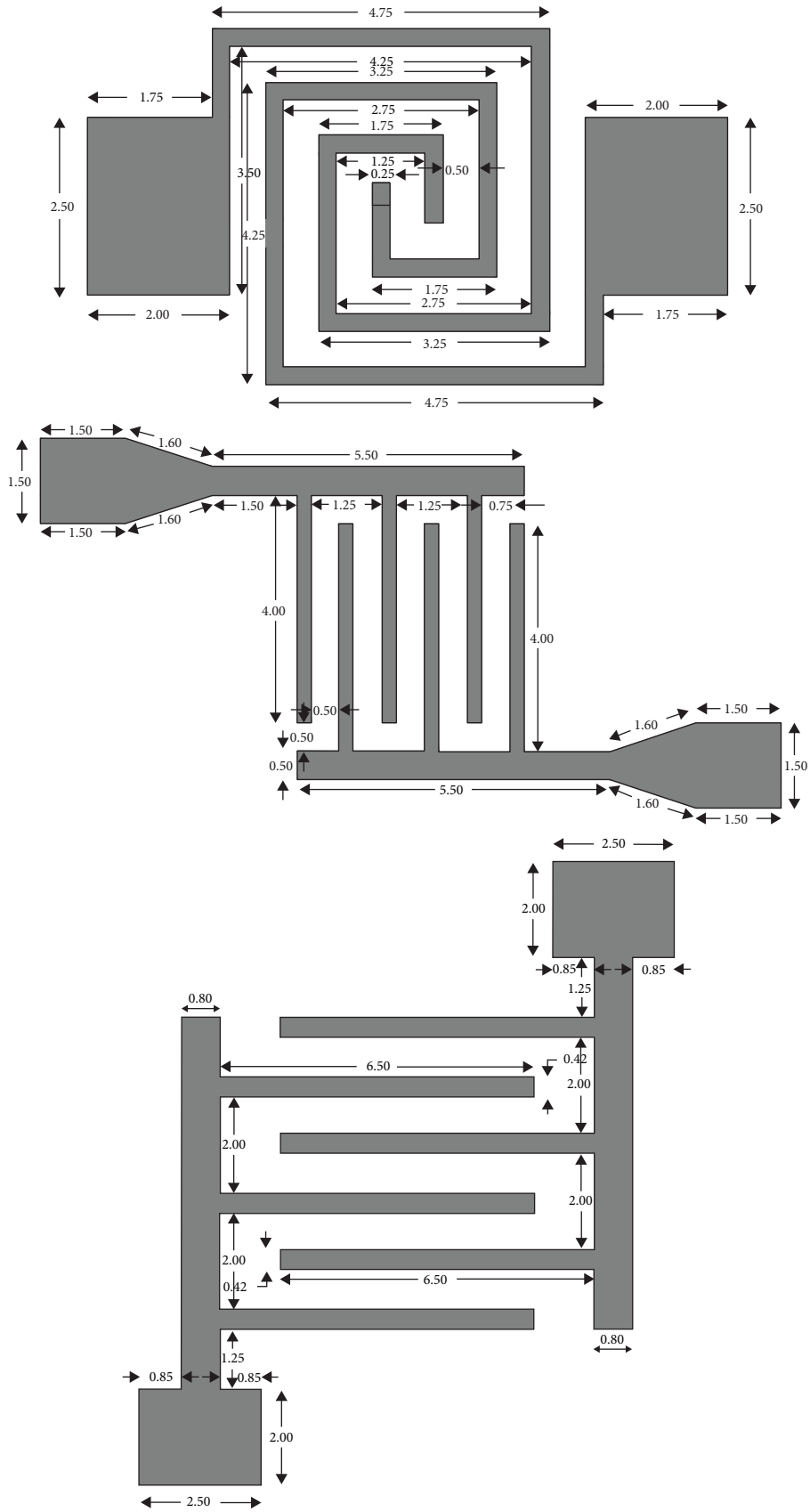

Figure 1: Three types of considered electrode patterns with their detailed dimensions (in mm).

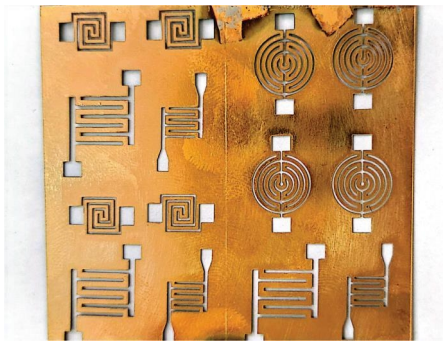

Figure 2: Fabricated mask.

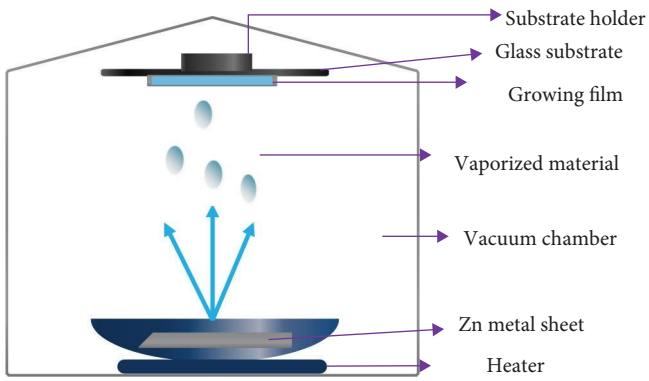

Figure 3: Schematic representation of the PVD coating process.

method. However, in this research, a simple and cheap alternative method is proposed.

2. Experimental Details

2.1. Electrode Design. Figure 1 shows the electrode patterns which are designed by Corel Draw software. These patterns were cut with a fiber laser on a 5 cm × 5 cm steel sheet, and the electrodes were deposited on the sample using this pattern.

2.2. Electrode Fabrication. Figure 2 corresponds to the fabricated mask. For each electrode deposition step, this mask is placed on the sample in the sputtering system, and gold is deposited on. The electrodes were coated onto the zinc oxide layer using the sputtering method with a power of 42 W and a thickness of 120 nm.

Finger distance, finger width, and effective area of A and B electrodes are equal to 500 μ, 250 μ, and 27.5 mm^2, respectively. Also, the finger distance, finger width, and effective area of the C electrode are equal to 800 μ, 400 μ, and 70.5 mm^2, respectively.

2.3. Materials and Methods. Before deposition, glass substrates were ultrasonically vibrated in acetone, ethanol, and distilled water for 15 min; after that, they were washed with deionized water and dried with airflow. The physical vapor deposition (PVD) method was employed to deposit ZnO on the substrate.

The PVD method is a process that takes place in a vacuum environment by applying electric current to evaporate the source material. The parameters that must be controlled in this type of deposition are chamber pressure and temperature of the plant where the source material is placed. The source material is used as a coating (such as a piece of metal) in a container, commonly referred to as a boat or filament, made of resistant metals which is placed in the container. By passing an electric current through the boat or filament and heating up the desired source material, it vaporizes in a vacuum environment. This vapor then forms a thin layer on the substrate due to the pressure difference between the container and the substrate. This technique involves heating a Zn source material in a vacuum chamber, causing the material to evaporate and deposit on the substrate. The deposition parameters, such as temperature and pressure, affect the film quality and its thickness. Figure 3 shows a schematic illustration of the PVD process. Here, 0.2 g of Zn is placed inside the chamber with the pressure of 2×10^{-5} bar, a filament current of 180 A, where it is placed in 13 cm of the substrate. The substrate temperature and the deposition time were set at about 150°C and 30 s, respectively. By heating the sample, it evaporated and the obtained vapor condensed on the substrate. Next, the sample was annealed for half an hour at the temperature of 500°C in an oxygen atmosphere with a flow rate of 200 sccm.

Next, 120 nm of gold was deposited on zinc oxide by direct sputtering. Then, two strands of copper wire were joined to the Au electrode using a conducting paste to make an electrical connection between the interdigitated electrode and Cu wire.

2.4. Sample Characterization. The X-ray diffraction (XRD) patterns were obtained using an X'pertPro device with a Cu Kα anode ($\lambda = 0.1542$ Å) operating at 40 kV and 30 mA. The diffraction patterns were generated with the step size of 0.05 (2θ) and the step time of 1 s. This device is manufactured by Panalytical Company in the Netherlands.

The crystalline size (D) was calculated using the Scherrer formula, $D = k\lambda/\beta\cos\theta$, where D is the particle diameter size, λ is the X-ray wavelength, β is the "full width at half maximum" (FWHM) of the sharp peaks, and θ is the angle. According to the mentioned explanations, the crystalline size is calculated to be 29.42 nm.

The field-emission scanning electron microscopy (FESEM) experiment is done by a MIRA3 TESCAN, where the acceleration voltage is in the range of 18–20 kV, the scan mode is 10 rate/min, and the beam current is 7 A.

3. Results and Discussion

3.1. Structural Properties. XRD stands for X-ray diffraction. This device emits X-rays at different angles to the sample and draws the result as a graph. In this diagram, a series of peaks can be seen, each peak corresponding to XRD from a specific atomic plane.

Figure 4 shows the XRD patterns of the pure Zn samples. The highest peak (002) is at 38.29°. The distinct diffraction peaks at 36.34°, 39.06°, 43.28°, and 77.04° diffraction angles correspond to the (002), (100), (101), and (004) plane, which

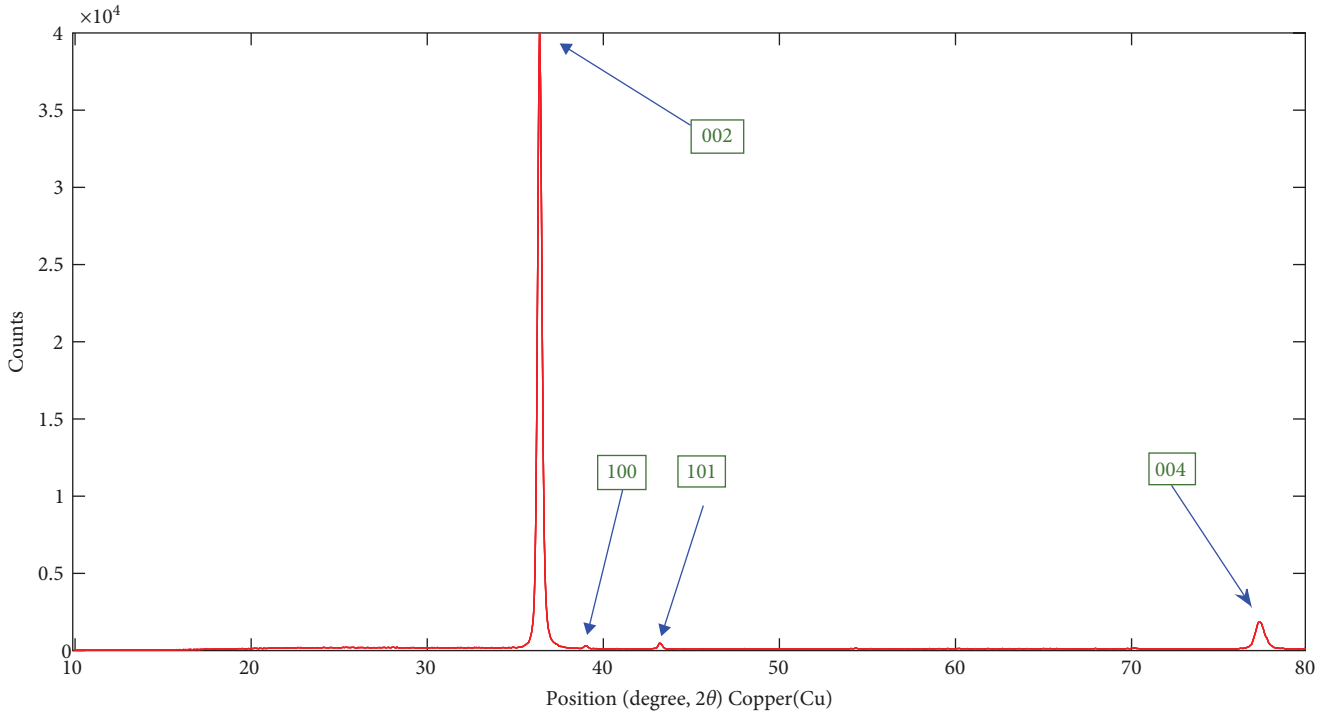

Figure 4: XRD patterns of the studied Zn sample before annealing.

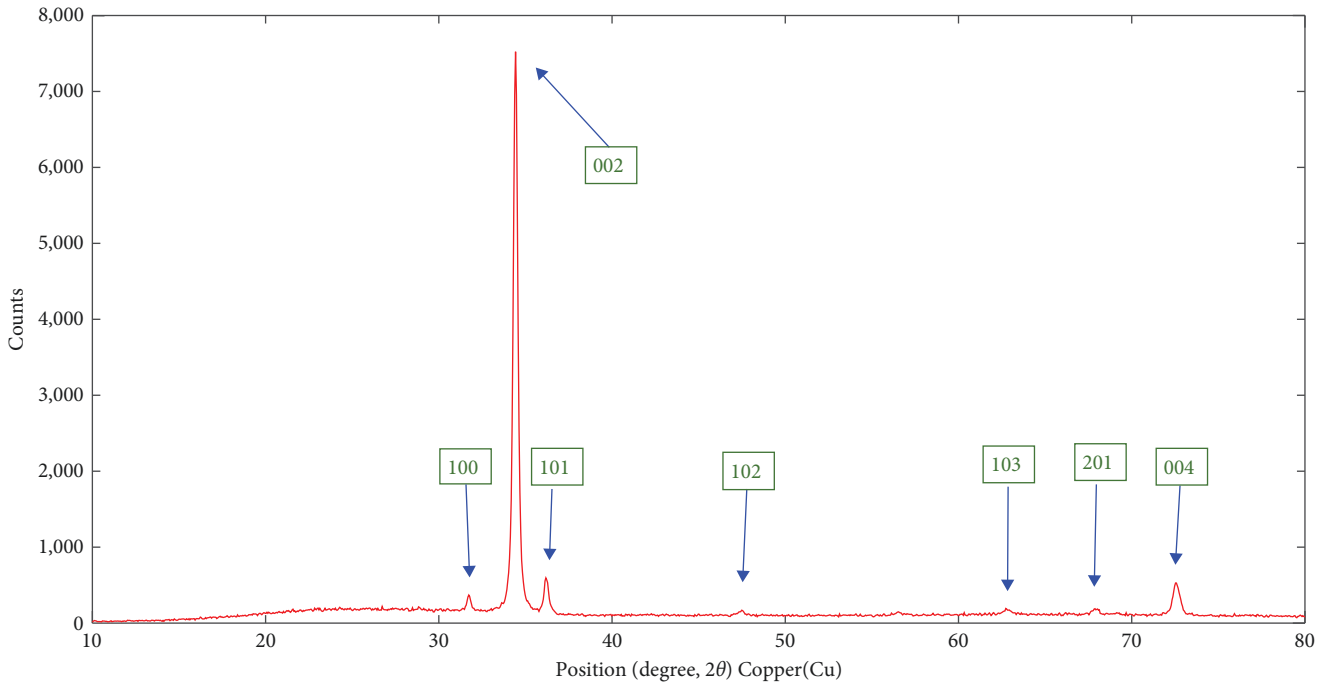

Figure 5: XRD patterns of the studied ZnO sample.

is characteristic of Zn material. Figure 5 shows the XRD pattern of the pure ZnO samples. The highest peak (002) at 34.46° confirms the growth direction of zinc oxide along the C axis [35]. As it is obvious from the XRD pattern, annealing leads to the improvement of crystallinity. The size of the crystal is calculated from the Debye–Sheerer relationship as 29.42 nm.

3.2. Surface Morphology Analysis. FESEM is a technique used to obtain high-resolution images of a sample surface with virtually unlimited depth of field while using an electron beam focused by electromagnetic lenses to scan the surface of a specimen, where the reflected/interacted electrons create an image of the sample surface and topography.

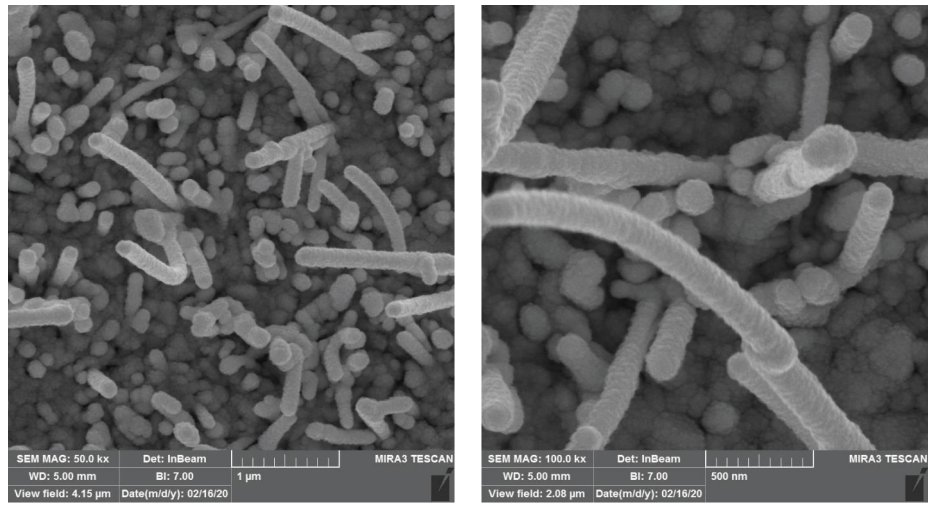

(a) (b)

Figure 6: FESEM images of the deposited layer in (a) 1 μm scale and (b) 500 nm scale.

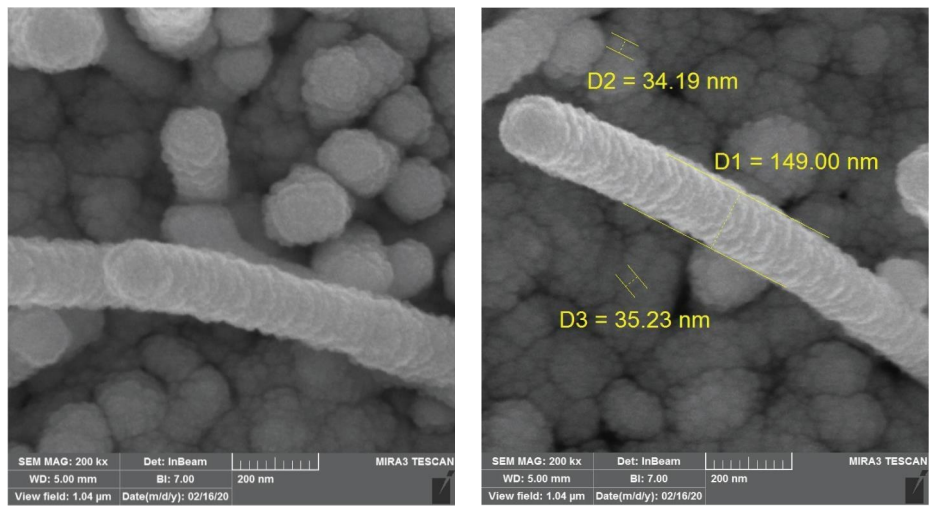

(a) (b)

Figure 7: (a) FESEM image of the deposited layer in 200 nm scale and (b) sample diameter.

Figures 6(a), 6(b), and 7(a) show the FESEM image of the ZnO layer synthesized by the PVD method in three scales of 1,000, 500, and 200 nm, respectively. As is apparent, the surface is composed of nanowires. Figure 7(b) shows the sample diameter. Also, the cross-sectional image indicates that the thickness of the layer is 405.46 nm.

3.3. Gas-Sensing Results. The testing structure of the fabricated gas sensor is illustrated in Figure 8. This structure consists of a gas inlet, gas outlet, temperature controller, and electrical data recording. The sensor was placed in the center of the chamber. After initial resistance was stabilized, ethanol vapors were injected into the gas chamber. To restore the sensor's resistance to its initial value, inert nitrogen gas is utilized, causing the release of ethanol vapor from its location. As a result, the resistance of the sample returns to its original state. The schematic of the fabricated gas sensor is shown at the corner of Figure 8. Also, the picture of the fabricated gas sensor is shown in Figure 9.

The results of sensing samples in the time domain are shown in Table 1. The sensitivity of the sensor is calculated using $S = [(R_g - R_a)/R_a] \times 100$, where R_a is the resistance of the sensor in the presence of the air ambient and R_g is the resistance of the sensor in the presence of the target gas.

Two important parameters of the gas sensors are their response time and recovery time. Response time is the time it takes for the sensor to detect the gas and produce a measurable signal, while recovery time is the time it takes for the sensor to return to its initial state after exposing to the target gas.

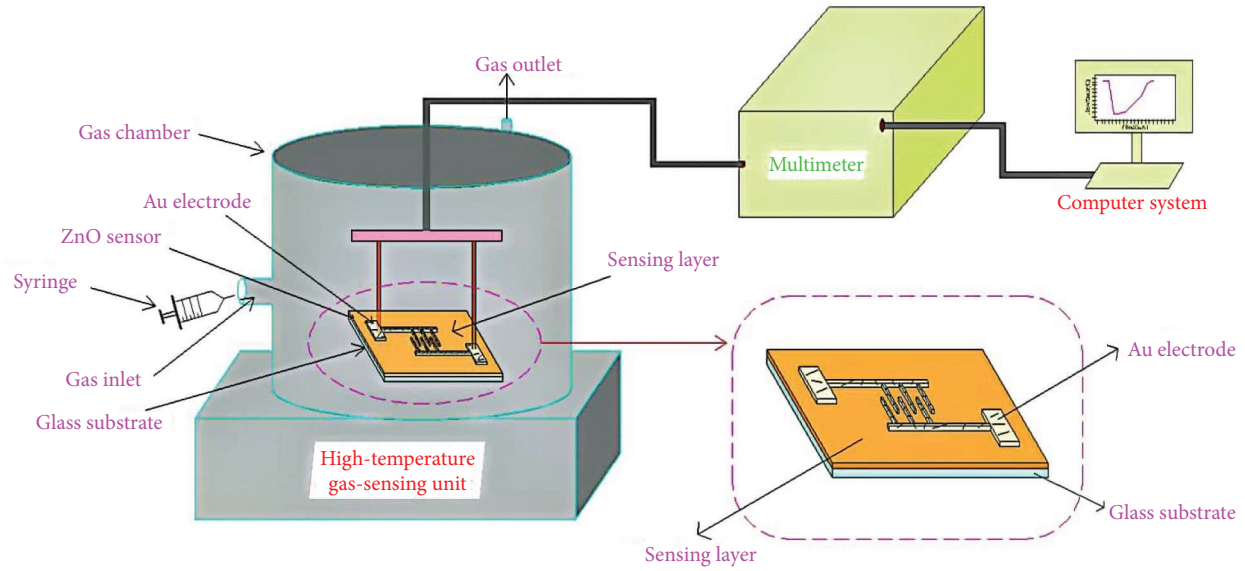

Figure 8: Schematic of gas-sensing procedure and the gas sensor structure.

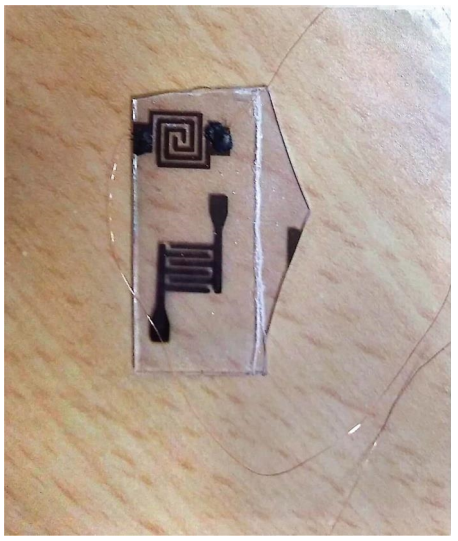

Figure 9: Fabricated gas sensor.

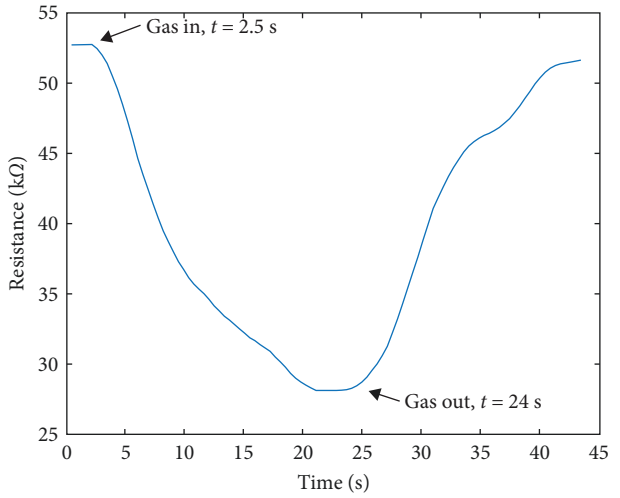

Figure 10: Transient response of A-sensor to 2,000 ppm ethanol concentration at 200°C.

Table 1: Sensing results of different electrode patterns.

Sample	Ethanol gas concentration (ppm)	Temperature (°C)	Sensitivity (%)	Response time (s)	Recovery time (s)
A	2,000	200	43	10	7.5
B	2,000	200	32	4	7.28
C	2,000	200	32	6	7.5
A	2,000	250	68	28.8	21
A	660	250	53	25	32
A	330	250	42	21	57

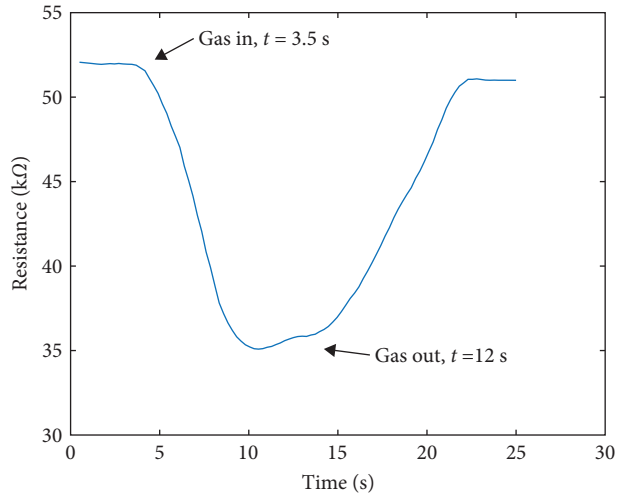

Figure 11: Response time of B-sensor to 2,000 ppm ethanol concentration at 200°C.

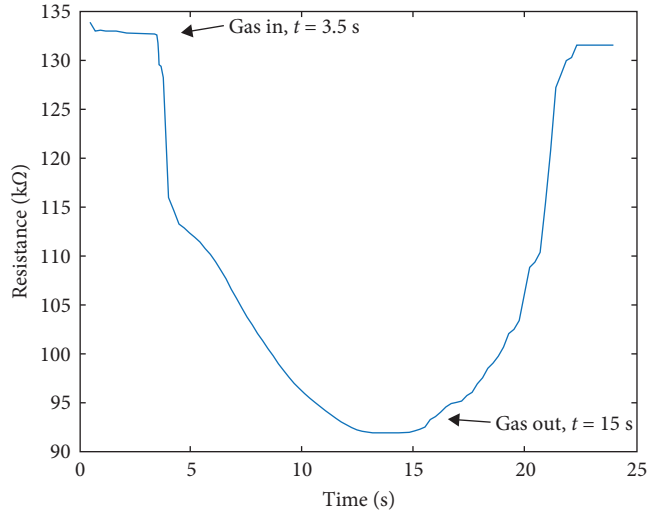

Figure 12: Response time of C-sensor to 2,000 ppm ethanol concentration at 200°C.

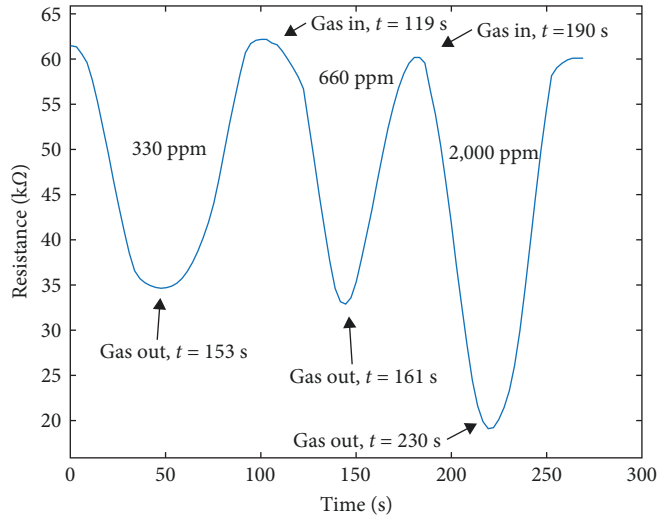

Figure 13: Response time of A-sensor at different ethanol concentrations at 250°C.

Table 2: Comparison of ZnO-based gas sensors.

Sensor structure	Sensor response time (s)	Response definition	Grain size (nm)	Temperature	Gas type
ZnO nanostructure [39]	5.8 (50 ppm)	R_{air}/R_{gas}	60	350°C	Ammonia
ZnO hollow sphere [40]	28 (200 ppm)	R_{air}/R_{gas}	5–8	400°C	Ammonia
ZnO nanorods [41]	40 (30 ppm)	I_{gas}/I_{air}	30–50	Room temperature	Ammonia
ZnO-nanowire [11]	12 (2,000 ppm)	R_{air}/R_{gas}	60–180	240°C	Ethanol
Au doped ZnO nanowires [11]	38 (200 ppm)	R_{air}/R_{gas}	15–25	240°C	Ethanol
This research	43 (2,000 ppm)	$(R_{gas}\text{-}R_{air})/R_{air}$	~35	200°C	Ethanol

The response and recovery times of a gas sensor can vary depending on the type and concentration of detected gas and also the sensor technology being used [36–38].

3.4. Gas-Sensing Mechanism. Considering that ZnO is an n-type semiconductor and ethanol is a reducing gas, in reaction with each other, they cause a drop in the resistance of the sensor. In this case, nitrogen is flushed inside the chamber for 4 min. Thus, the resistance returns to its initial value.

Figures 10–12 show the dynamic resistance transient of the sensors fabricated for A, B, and C electrodes, respectively, toward 2,000 ppm of ethanol at 200°C. The comparison of the three sensors demonstrates that the sensitivity of the square-spiral electrode is higher than that of the comb electrode. This is because the area between fingers in the square-spiral and small comb electrodes is 13.25 and 12 mm^2, respectively, let the absorption of more molecules and larger current for square-spiral electrode shape. In other words, it can be mentioned that for resistive sensors, the effect of interelectrode distance plays a more effective role than finger width. The sensitivity of the sensor fabricated using a C electrode with an effective area of 70.5 mm^2 has not changed compared to the B sensor with an effective area of 27.5 mm^2. Because in sample C, both width and inter-electrode distance parameters have changed simultaneously [18, 23]. For these two sensors, the ratio of width to finger distance has not changed, so the sensitivity has remained constant. Also, by increasing the inter-electrode distance, the initial resistance of sensor C has increased compared to sensor B. In comb electrodes, changing the width-to-finger distance ratio leads to a small increment in sensor sensitivity. In addition, the recovery time in all three electrode shapes remains almost constant, which shows that the recovery time is independent of the electrode geometry. The response time of the comb electrode is less than the square-spiral type. Therefore, depending on the application where sensitivity or response time is important, the optimal mode should be selected. Considering Figure 13, the sensitivity of sample A increased with increasing temperature and concentration of ethanol vapor from 330 to 2,000 ppm. Table 2 presents a summarized comparison between our research and other reported works for ZnO-based gas sensors.

4. Conclusion

In this work, the zinc (Zn) thin film has been prepared by the PVD method. Then, an annealing process was employed to grow the ZnO nanowire layer. Surface morphologies were characterized using SEM, which revealed nanowire shape. In addition, XRD analysis demonstrated that ZnO nanowire possessed a wurtzite structure with an orientation of (002). Totally, three types of sensors with different electrode geometries were designed, fabricated, and tested for their ethanol vapor-sensing properties. Based on the provided results, the sensor with square-spiral electrodes showed the sensitivity of 43% and 68% at 200 and 250°C, respectively, which is the highest value in comparison with other electrodes. For this shape of the electrode, a larger area is involved in the sensing process, thus the sensitivity is increased. The response time of the comb electrode is faster than the square-spiral electrode, while the recovery time is almost independent of the electrode geometry. Two sensors with comb electrodes and different dimensions showed the same sensitivity; as for the large comb electrode, both the finger width and distance have changed simultaneously.

Data Availability

We have not used any data to support the results of our study.

Conflicts of Interest

The authors declare that they have no conflicts of interest.

References

[1] P. S. Venkatesh, P. Dharmaraj, V. Purushothaman, V. Ramakrishnan, and K. Jeganathan, "Point defects assisted NH_3 gas sensing properties in ZnO nanostructures," *Sensors and Actuators B: Chemical*, vol. 212, pp. 10–17, 2015.

[2] D. Lun and K. Xu, "Recent progress in gas sensor based on nanomaterials," *Micromachines*, vol. 13, no. 6, Article ID 919, 2022.

[3] M. Aleksanyan, A. Sayunts, G. Shahkhatuni, Z. Simonyan, G. Shahnazaryan, and V. Aroutiounian, "Gas sensor based on ZnO nanostructured film for the detection of ethanol vapor," *Chemosensors*, vol. 10, no. 7, Article ID 245, 2022.

[4] Q. Li, D. Chen, J. Miao et al., "Highly sensitive sensor based on ordered porous ZnO nanosheets for ethanol detecting application," *Sensors and Actuators B: Chemical*, vol. 326, Article ID 128952, 2021.

[5] Y. Deng, "Applications of semiconducting metal oxide gas sensors," in *Semiconducting Metal Oxides for Gas Sensing*, pp. 325–385, Springer, Singapore, 2023.

[6] Y. Song, F. Chen, Y. Zhang et al., "Fabrication of highly sensitive and selective room-temperature nitrogen dioxide sensors based on the ZnO nanoflowers," *Sensors and Actuators B: Chemical*, vol. 287, pp. 191–198, 2019.

[7] P. Raju and Q. Li, "Review—semiconductor materials and devices for gas sensors," *Journal of the Electrochemical Society*, vol. 169, no. 5, Article ID 057518, 2022.

[8] S. Durrani, "The influence of electrode metals and its configuration on the response of tin oxide thin film CO sensor," *Talanta*, vol. 68, no. 5, pp. 1732–1735, 2006.

[9] M. Suchea, S. Christoulakis, K. Moschovis, N. Katsarakis, and G. Kiriakidis, "ZnO transparent thin films for gas sensor applications," *Thin Solid Films*, vol. 515, no. 2, pp. 551–554, 2006.

[10] F. Cao, C. Li, M. Li, H. Li, X. Huang, and B. Yang, "Direct growth of Al-doped ZnO ultrathin nanosheets on electrode for ethanol gas sensor application," *Applied Surface Science*, vol. 447, pp. 173–181, 2018.

[11] N. Hongsith, C. Viriyaworasakul, P. Mangkorntong, N. Mangkorntong, and S. Choopun, "Ethanol sensor based on ZnO and Au-doped ZnO nanowires," *Ceramics International*, vol. 34, no. 4, pp. 823–826, 2008.

[12] S. Jaballah, M. Benamara, H. Dahman et al., "Effect of Mg-doping ZnO nanoparticles on detection of low ethanol concentrations," *Materials Chemistry and Physics*, vol. 255, Article ID 123643, 2020.

[13] S. Bhatia, N. Verma, and R. K. Bedi, "Ethanol gas sensor based upon ZnO nanoparticles prepared by different techniques," *Results in Physics*, vol. 7, pp. 801–806, 2017.

[14] L. Piliai, D. Tomeček, M. Hruška et al., "New insights towards high-temperature ethanol-sensing mechanism of ZnO-based chemiresistors," *Sensors*, vol. 20, no. 19, Article ID 5602, 2020.

[15] L. Zhu and W. Zeng, "Room-temperature gas sensing of ZnO-based gas sensor: a review," *Sensors and Actuators A: Physical*, vol. 267, pp. 242–261, 2017.

[16] X. Yu, X. Chen, X. Ding, K. Tang, X. Zhao, and F. Liu, "Room temperature ethanol sensor based on ZnO nanoparticles modified by WSe_2 nanosheets," *Sensors and Actuators B: Chemical*, vol. 382, Article ID 133530, 2023.

[17] J. Qi, H. Zhang, S. Lu, X. Li, M. Xu, and Y. Zhang, "High performance indium-doped ZnO gas sensor," *Journal of Nanomaterials*, vol. 2015, Article ID 954747, 6 pages, 2015.

[18] S. Lee, "Electrodes for semiconductor gas sensors," *Sensors*, vol. 17, no. 4, Article ID 683, 2017.

[19] S. Saukko and V. Lantto, "Influence of electrode material on properties of SnO_2-based gas sensor," *Thin Solid Films*, vol. 436, no. 1, pp. 137–140, 2003.

[20] M. Toohey, "Electrodes for nanodot-based gas sensors," *Sensors and Actuators B: Chemical*, vol. 105, no. 2, pp. 232–250, 2005.

[21] S. J. Ikhmayies, N. M. Abu El-Haija, and R. N. Ahmad-Bitar, "A comparison between different ohmic contacts for ZnO thin films," *Journal of Semiconductors*, vol. 36, no. 3, Article ID 033005, 2015.

[22] V. R. Naganaboina, S. Bonam, M. Anandkumar, A. S. Deshpande, and S. G. Singh, "Improved chemiresistor gas sensing response by optimizing the applied electric field and interdigitated electrode geometry," *Materials Chemistry and Physics*, vol. 305, Article ID 127975, 2023.

[23] P. Y. P. Adelyn, U. Hashim, M. K. M. Arshad et al., "Fabrication and characterization on width of spiral interdigitated electrodes based biosensors," *AIP Conference Proceedings*, vol. 1808, no. 1, Article ID 020039, 2017.

[24] C.-C. Lin, P.-L. Hsu, L. Lin, and J.-G. Hwu, "Investigation on edge fringing effect and oxide thickness dependence of inversion current in metal-oxide-semiconductor tunneling diodes with comb-shaped electrodes," *Journal of Applied Physics*, vol. 115, Article ID 124109, 2014.

[25] P. Durina, T. Plecenik, M. Mosko et al., "Properties of metal oxide gas sensors with electrodes placed below the sensing layer," *Key Engineering Materials*, vol. 605, pp. 527–530, 2014.

[26] A. A. Haidry, E. Çiftyürek, and B. Saruhan, "Low temperature gas sensing with novel top-bottom electrode configuration," *Procedia Engineering*, vol. 120, pp. 245–248, 2015.

[27] C.-M. Yang, T.-C. Chen, Y.-C. Yang, M. Meyyappan, and C.-S. Lai, "Enhanced acetone sensing properties of monolayer graphene at room temperature by electrode spacing effect and UV illumination," *Sensors and Actuators B: Chemical*, vol. 253, pp. 77–84, 2017.

[28] T.-Y. Chen, H.-I. Chen, C.-S. Hsu et al., "ZnO-nanorod-based ammonia gas sensors with underlying Pt/Cr interdigitated electrodes," *IEEE Electron Device Letters*, vol. 33, no. 10, pp. 1486–1488, 2012.

[29] D. D. Le, T. N. N. Nguyen, D. C. T. Doan, T. M. D. Dang, and M. C. Dang, "Fabrication of interdigitated electrodes by inkjet printing technology for apllication in ammonia sensing," *Advances in Natural Sciences: Nanoscience and Nanotechnology*, vol. 7, no. 2, Article ID 025002, 2016.

[30] Y. N. Wu, T. Jiang, T. L. Shi, B. Sun, Z. R. Tang, and G. L. Liao, "Au modified ZnO nanowires for ethanol gas sensing," *Science China Technological Sciences*, vol. 60, no. 1, pp. 71–77, 2017.

[31] K. G. Saw, S. S. Tneh, G. L. Tan et al., "Ohmic-rectifying conversion of Ni contacts on ZnO and the possible determination of ZnO thin film surface polarity," *PLOS ONE*, vol. 9, no. 1, Article ID e86544, 2014.

[32] L. J. Brillson and Y. Lu, "ZnO schottky barriers and ohmic contacts," *Journal of Applied Physics*, vol. 109, no. 12, Article ID 121301, 2011.

[33] C.-J. Chang, C.-Y. Lin, J.-K. Chen, and M.-H. Hsu, "Ce-doped ZnO nanorods based low operation temperature NO_2 gas sensors," *Ceramics International*, vol. 40, no. 7, pp. 10867–10875, 2014.

[34] C.-J. Chang, J.-K. Chen, and T.-L. Yang, "Cr-doped ZnO based NO_2 sensors with high sensitivity at low operating temperature," *Journal of the Taiwan Institute of Chemical Engineers*, vol. 45, no. 4, pp. 1876–1882, 2014.

[35] A. Khan, M. Hussain, M. A. Abbasi, Z. H. Ibupoto, O. Nur, and M. Willander, "Study of transport properties of copper/zinc-oxide-nanorods-based Schottky diode fabricated on textile fabric," *Semiconductor Science and Technology*, vol. 28, no. 12, Article ID 125006, 2013.

[36] S.-Y. Bak, J. Lee, Y. Kim et al., "Sensitivity Improvement of urchin-like ZnO nanostructures using two-dimensional electron gas in MgZnO/ZnO," *Sensors*, vol. 19, no. 23, Article ID 5195, 2019.

[37] K. He, Z. Jin, X. Chu et al., "Fast response–recovery time toward acetone by a sensor prepared with Pd doped WO_3 nanosheets," *RSC Advances*, vol. 9, no. 49, pp. 28439–28450, 2019.

[38] A. Ponzoni, "A statistical analysis of response and recovery times: the case of ethanol chemiresistors based on pure SnO_2," *Sensors*, vol. 22, no. 17, Article ID 6346, 2022.

[39] Y. Zeng, Z. Lou, L. Wang et al., "Enhanced ammonia sensing performances of Pd-sensitized flowerlike ZnO nanostructure," *Sensors and Actuators B: Chemical*, vol. 156, no. 1, pp. 395–400, 2011.

[40] F. Meng, J. Yin, Y.-Q. Duan, Z.-H. Yuan, and L.-J. Bie, "Co-precipitation synthesis and gas-sensing properties of ZnO hollow sphere with porous shell," *Sensors and Actuators B: Chemical*, vol. 156, no. 2, pp. 703–708, 2011.

[41] N. Du, H. Zhang, B. Chen, J. Wu, and D. Yang, "Low-temperature chemical solution route for ZnO based sulfide coaxial nanocables: general synthesis and gas sensor application," *Nanotechnology*, vol. 18, no. 11, Article ID 115619, 2007.